

Temperature Dependent Failure of Atomically Thin MoTe₂

A S M Redwan Haider^{1#}, Ahmad Fatehi Ali Mohammed Hezam^{1#}, Md Akibul Islam^{2}, Rafsan Al Shafatul Islam Subad³, Yeasir Arafat⁴, Mohammad Tanvirul Ferdous⁴, Sayedus Salehin^{1*}, Md.Rezwanul Karim^{1*}*

¹Department of Mechanical and Production Engineering, Islamic University of Technology, Bangladesh.

²Department of Mechanical and Industrial Engineering, University of Toronto, Canada.

³Department of Mechanical Engineering, University of Massachusetts-Dartmouth, USA.

⁴Independent Researcher.

[#]Equal Contributions

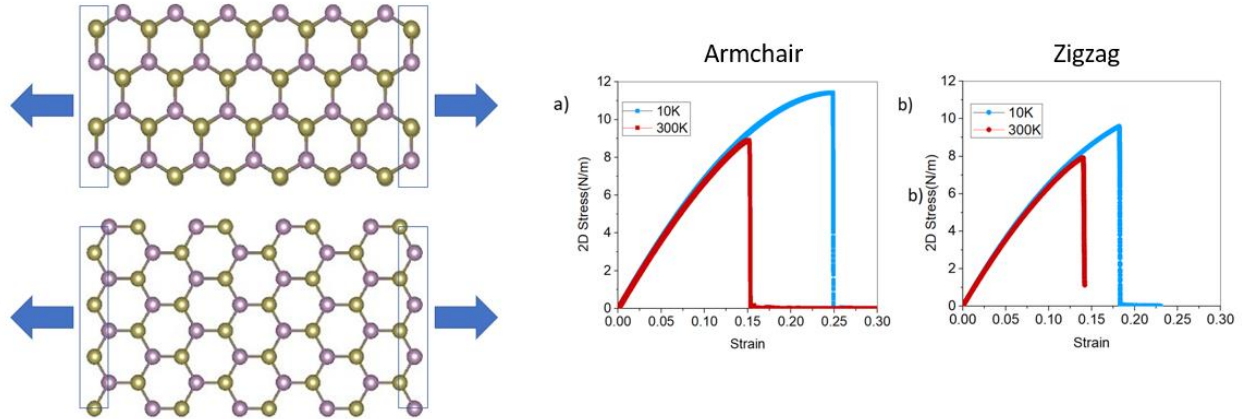
^{*}Corresponding Authors

Abstract:

In this study, we systematically investigated the mechanical response of monolayer molybdenum ditelluride (MoTe₂) using molecular dynamics simulations. The tensile behavior of trigonal prismatic phase (2H phase) MoTe₂ under uniaxial strain was simulated in the armchair and zigzag direction. We also investigated the crack formation and propagation in both armchair and zigzag directions at 10K and 300K to understand the fracture behavior of monolayer MoTe₂. The crack simulations show clean cleavage for the armchair direction and the cracks were numerous and scattered in the case of the zigzag direction. Finally, we investigated the effect of temperature on Young's modulus and fracture stress of monolayer MoTe₂. The results show that at a strain rate of 10^{-4} ps⁻¹, the fracture strength of 2H-MoTe₂ in the armchair and zigzag direction at 10K is 16.33 GPa (11.43 N/m) and 13.71429 GPa (9.46 N/m) under a 24% and 18% fracture strain, respectively. The fracture strength of 2H-MoTe₂ in the armchair and zigzag direction at 600K is 10.81 GPa (7.56 N/m) and 10.13 GPa (7.09 N/m) under a 12.5% and 12.47% fracture strain, respectively. Although experimental results on MoTe₂ are limited for a wide range of temperatures, we have found that young's modulus agrees with results with existing literature for pristine MoTe₂. For

2H-MoTe₂ in both armchair and zigzag directions, the fracture stresses, fracture strengths, and Young's modulus fall as the temperature rises, resulting from the increased atomic thermal vibrations.

Graphical Abstract:



Keywords: 2D materials, molybdenum ditelluride, molecular dynamics, Stillinger Weber potential, Fracture mechanics.

.....

1. Introduction

Since the discovery of graphene in 2004[1], atomically thin two-dimensional materials have attracted great interest due to their excellent mechanical[2], electrical[3], thermal [4], optical [5], and magnetic properties[6]. However, graphene exhibits a zero-band gap in its structure making it difficult to use in transistor applications [1] and bioelectronics [7] . Transition metal dichalcogenides (TMDCs) hence emerged as a promising candidate for transistor applications due to the presence of direct and indirect band gap in their structure[8]–[10]. A TMDC is a sandwich structure where a metal atom (M) is sandwiched between two chalcogen atoms (X) in hexagonal layers and is represented as MX_2 . Group VI TMDCs (Mo and W) are of particular interest due to more than one possible 2D crystal structure. One of these structural phases is semiconducting and the other one is metallic [11]–[13]. This is an interesting property since the semiconducting phase can be used to make electronic devices[11] and the metallic phase can be used in catalytic activities leading to hydrogen evolution[14]–[16]. It has been suggested in the literature that the phase transition between the semiconducting and metallic phases is possible using controlled strain[17]. Among all the TMDCs, MoS_2 has received the most attention in this aspect. However, MoS_2 may not be the best candidate for strain-induced phase transition due to the high energy required for the transition ($\Delta E > 0.8 \text{ eV}$)[17]. In contrast, MoTe_2 exhibits a significantly smaller energy difference between its semiconducting and metallic phase ($\Delta E < 50 \text{ meV}$) [17], [18]. Hence, it is of utmost importance to investigate the mechanical properties of monolayer MoTe_2 under controlled strain to determine the stability and durability of this TMDC. Here, we focus on the 2H phase of MoTe_2 which exhibits Si -like indirect bandgap ($\sim 1 \text{ eV}$)[19]. MoTe_2 has recently been used in a wide range of applications ranging from photodetectors [20], and energy storage [21] to novel piezoelectricity [22]. Among all the TMDCs, molybdenum ditelluride (MoTe_2) has attracted special attention due to the possibility of phase transition between two stable phases- semiconducting 2H (hexagonal; $\sim 1 \text{ eV}$ bandgap) and metallic 1T (octahedral)[18], [23]–[25]. The first principal energy calculations revealed that MoTe_2 has a smaller energy difference between 2H and 1T phases than other TMDCs. The literature has reported that monolayer 2H- MoTe_2 can be phase transitioned to 1T- MoTe_2 using only 3% strain [17]. This paves the way for the low energy transition between semiconducting and metallic phase which can be useful in-memory applications. The impact of incorporating a 10 vol% proportion of MoTe_2 nanostructures in the PBDB-T: ITIC polymer matrix as the active layer for developing solar cells and photodetector

devices indicated that the highest power conversion efficiency of approximately 8.94% was achieved [26]. Another fascinating property of monolayer MoTe₂ is its flexibility and stretchability, making it possible to apply external deformation to manipulate their physical properties [27]. Atomic force microscopy (AFM) has been recently used to demonstrate the phase transition in MoTe₂ using the nanoindentation method[28]. However, due to the instability of MoTe₂ in ambient air[29], it is difficult to conduct a detailed study on the phase transition and the mechanics of monolayer MoTe₂. Due to this difficulty, the literature on monolayer MoTe₂ mechanics in ambient air is still elusive. Molecular dynamics offers a unique opportunity to perform experiments on the 2D MoTe₂ in an environment that prevents it from exposing to air. Multiple simulations can be conducted on the same material to predict the outcome before performing hands-on experiments. Therefore, computer simulations reduce the cost of random experimentation. However, it is worth mentioning that atomic force microscopy (AFM) based nanoindentation techniques have been used to measure the elastic properties of a few layers of MoTe₂ [27] and not the monolayers which are of most interest. The response of 2H, 1T, and 1T'-MoTe₂ to uniaxial tensile conditions was investigated using DFT. Initially, these 2D layers demonstrated a linear response, which was followed by a non-linear trend up to the ultimate tensile stress [30] .

The unique mechanical properties of two-dimensional (2D) materials make them a fascinating subject for study in the field of fracture mechanics, as their behavior under stress and strain can differ significantly from that of their three-dimensional counterparts [31]. The purpose of this work is to discuss the deformation and fracture behavior of monolayer 2H-MoTe₂ at a wide range of temperatures. To precisely mimic the mechanical properties of MoTe₂ using an SW interatomic potential, we first developed parameterization of the potential. Then we applied uniaxial strain [32] using molecular dynamic (MD) simulation along the zigzag and armchair direction till the monolayer fails. Analysis of stress-strain responses beyond the linear elastic regime reveals directional anisotropy in mechanical behaviour and failure qualities. Finally, we varied the temperature from 100K to 600K to investigate the elastic and failure properties in monolayer 2H-MoTe₂.

One of the stable phases of monolayer MoTe₂ is the 2H phase, as shown in Figure 1. Here hexagonally arranged, each molybdenum atom is sandwiched between two layers of tellurium

atoms forming a Te-Mo-Te sequence. Each Mo atom has six Te atoms as its first neighbors, and each Te atom is directly bound to three Mo atoms in the trigonal prismatic coordination of the intralayer atoms (Mo and Te atoms within a single layer) as shown in figure 1. Te and Mo are bonded by strong covalent bonds. The covalent bonds are predominantly governed by three bond-stretching (Mo-Te, Mo-Mo, and Te-Te) and three angle-bending motions (two Mo-Te-Te angles with Mo being the central atom and one Te-Mo-Mo). For the convenience of creating the structures in MD, we used a hexagonal unit cell ($a=b=3.159$ and $c=13.964$ $\alpha=\beta=90$ deg and $\gamma=120$ deg [33]).

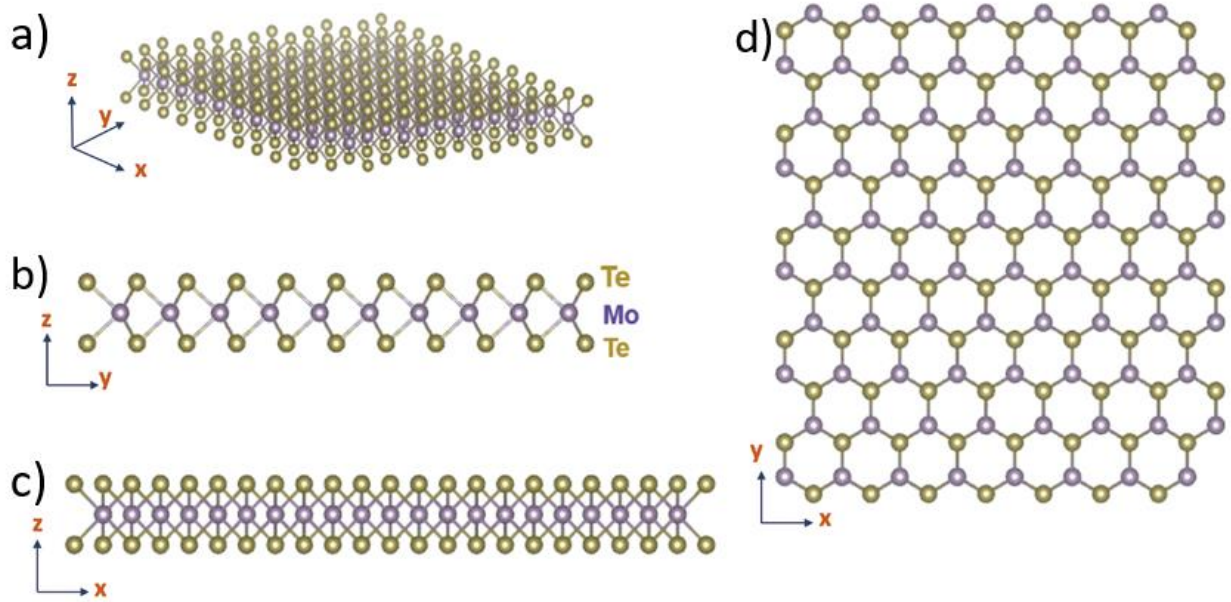


Figure 1: The crystal structure of monolayer MoTe₂ showing a layer of molybdenum atoms (purple) sandwiched between two layers of Tellurium atoms (olive). a) Orthogonal View, b) Front View, c) Side View and d) Top View.

2. Computational Method

In the following section, we introduce the simulator software that was used to perform the simulations along with the essential working conditions and environment that were required to run the simulation. The description of the MoTe₂ structure that was used is also provided describing the bond lengths, angles and total dimensions of the sheet. Additionally, the governing equations of the model are provided.

2.1 Modelling monolayer 2H-MoTe₂

LAMMPS (*Large-scale Atomic/Molecular Massively Parallel Simulator*) is a simulator that runs using Molecular dynamics simulation code [34]. It can model Nano-scale to macroscopic systems using various atomic potentials and boundary conditions. In our work, Stillinger–Weber (SW) potential is used [35], which describes the interaction of atoms inside a TMD and the coupling between them. SW potential parameters are parameterized for different materials[36] to develop a better SW potential, since it provides a more accurate mechanical behavior and phonon spectrum. This is done by modification of LAMMPS using CMake to incorporate experimentally known values[36]. CMake is an open-source tool that can be used to build different source codes. It is normally used for C and C++ languages; however, it can also be used for other languages too. There are two inequivalent bond angles in any hexagonal molybdenum dichalcogenides unit cell. Since the values are very close, a single bond angle is considered for simplification of the calculation. The modification gives a reasonably accurate result for MoS₂ [36] thus also applicable for similar MX₂ materials. After the modification, Jiang et al [36] tested the strain-induced buckling on a composite TMD heterostructure. The modified code uses a bending angle of $\theta=80.581^\circ$ for all TMDs.

The MoTe₂ structure has a Molybdenum (Mo) connected to a trigonal prism of six tellurium. The bond length of Mo-Te is approximately taken as 2.73 Å. Each Tellurium (Te) is surrounded by ten other Te atoms. Six Te atoms have a bond length of 3.52 Å in plane (001), one directly below is at 3.63 Å and three above it is at 3.92 Å. The bond angles of Te-Mo-Te are 83.5°, 80.4° and 133.9°. However, due to the parameterization of SW potential the two inequivalent bond angles are taken as equal 80.581[37]. We used a 30 nm X 30 nm large sheet for this simulation.

2.2 Stress-strain relation and distribution

Atomic stress-strain behavior is obtained by deforming the simulation box uniaxially and calculating the average stress over the structure. Atomic stress was calculated based on the definition of virial stress. Virial stress components are calculated using [38], [39]:

$$\sigma_{\text{Virial}}(r) = \frac{1}{\Omega} \sum_i [(-m_i \dot{u}_i \otimes \dot{u}_i + \frac{1}{2} \sum_{j \neq i} r_{ij} \otimes f_{ij})] \quad (1)$$

The summation is upon all the atoms in the total volume Ω , m_i is the atomic mass i , \dot{u}_i is the time derivative which indicates the displacement of atom concerning a reference position, r_{ij} is the position vector of atom, \otimes is the cross product, and f_{ij} is the interatomic force applied on atom i by atom j . Here, in this study, the Stillinger-weber (SW) potential was used to define the interatomic interactions[35]. The SW potential comprises two-body and three-body terms describing bond stretching and breaking.

The mathematical expressions used to calculate the components of the virial stress:

$$\phi = \sum_{i < j} V_2 + \sum_{i > j < k} V_3 \quad (2)$$

$$V_2 = A e^{\left[\frac{\rho}{r - r_{max}} \right]} \left(\frac{B}{r^4} - 1 \right) \quad (3)$$

$$V_3 = K \epsilon e^{\frac{\rho_1}{r_{ij} - r_{maxij}} - \frac{\rho_2}{r_{ik} - r_{maxik}}} (\cos \cos \theta - \cos \cos \theta_0)^2 \quad (4)$$

Here V_2 , and V_3 are the two-body bond stretching and angle bending terms accordingly. The terms r_{max} , r_{maxij} , r_{maxik} are cut-off ratios and θ_0 at the equilibrium configuration is the in-between angle of the two bonds. A and K are energy-related parameters based on the Valence Force Field (VFF) model. B, ρ, ρ_1 and ρ_2 are other parameters that are fitted coefficients. A and K are two energy parameters. Such parameters along with the corresponding values, were extracted from Li et al [40] .

The LAMMPS code uses these following equations to calculate the required data.

The stress can be calculated using:

$$\sigma = \frac{P_{xx} * L_y * L_z}{L_{y0} * L_{z0}} \quad (5)$$

P_{xx} is the Tensile load

The strain can be calculated using:

$$\epsilon = \frac{L_x - L_{x0}}{L_{x0}} \quad (6)$$

L_x is the instantenous length of MoTe2 along x – axis.

L_{x0} is the undeformed length of MoTe2 along x – axis.

The stress produced was divided by this number to calculate the plane stress using:

$$Plane\ Stress = \frac{Stress}{thickness} \quad (7)$$

3. Results

In order to investigate the fracture process in the 2H-MoTe₂, we subjected the sheet under uniaxial tension from both ends in the simulation and increased the strain until the sheet completely fractures. We used 10K and 300K temperature initially to understand the effect of temperature on the fracture behavior of the 2D sheet. At 10K, we strained the 2D MoTe₂ along the armchair and zigzag edges from 0% to 24.83% and the stress in the 2D MoTe₂ increases from 0 to ~12 GPa. Although the entire sample surface is subjected to uniform tension deformation, thermal variations at the limited temperature cause the atomic stresses not to be distributed uniformly.

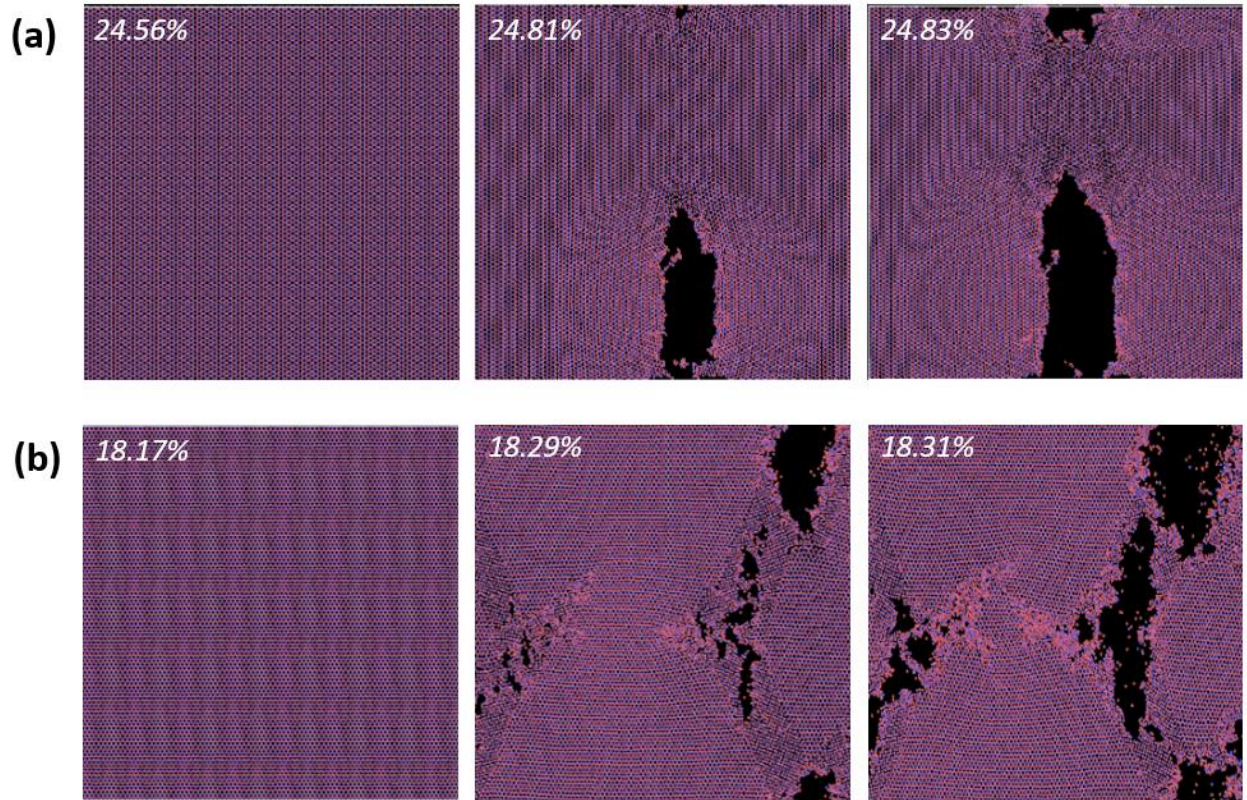


Figure 2: Crack nucleation and propagation in 2D MoTe₂ along the (a) armchair and (b) zigzag edges at 10K

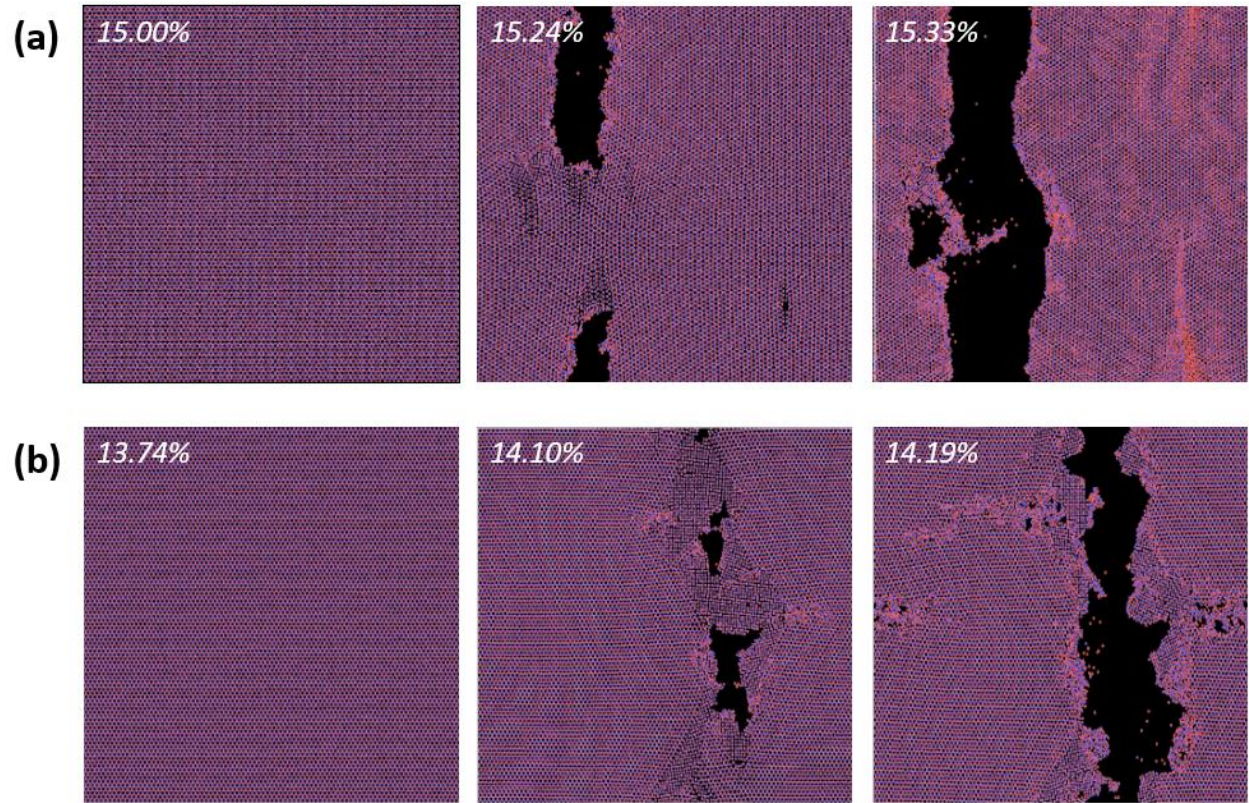


Figure 3: Crack nucleation and propagation in 2D MoTe₂ along the (a) armchair and (b) zigzag edges at 300K

It is observed in Figure 2(a) that along the armchair direction, a small crack starts to nucleate at 24.81% strain by breaking of atomic bonds. The crack starts to propagate as the strain is increased without showing any sign of plasticity in the 2D sheet. The sheet does not fail completely, even at 24.83% strain. A similar characteristic is observed along the zigzag edges at 10K temperature Figure 2(b). We increased the strain from 0% to 18.31% and the stress in the 2D sheet increased from 0 to ~10 GPa. A small crack starts to nucleate at 18.17% strain which starts a brittle failure, and the sheet completely fails at 18.31% strain. It is to be noted that, unlike the armchair edge, the fracture along the zigzag edge was not a clean cleavage. This shows that the fracture preferentially along a puckered groove for loads in the armchair direction rather than across the grooves. Additionally, the fracture occurred at a lower strain along the zigzag edge than the armchair edge. Afterwards, we increased the temperature to 300K and applied a similar uniaxial strain on the 2D MoTe₂ sheet along the armchair and zigzag edge as shown in Figure 3. For the armchair direction, the crack started to nucleate at 15.2% strain and then cleaved suddenly into two clean pieces at

15.33% strain (Figure 3a). This is indicative of the same brittle behavior as before at elevated temperatures. The fracture 2D stress recorded was ~ 8.5 N/m. However, in the zigzag direction, the crack started to nucleate at 14.1% strain and failed at 14.19%. The fracture 2D stress was recorded at ~ 8 N/m (Figure 3b). In both figures 2 and 3 rippling were observed due to the bucking of outer Te layers. Since the poison's ratio is positive, when the 2D sheet is stretched in one-side it produces a compression on the other direction. Therefore, the compression leads to a bucking effect. The stress-strain relations of both edges are shown in Figure 4.

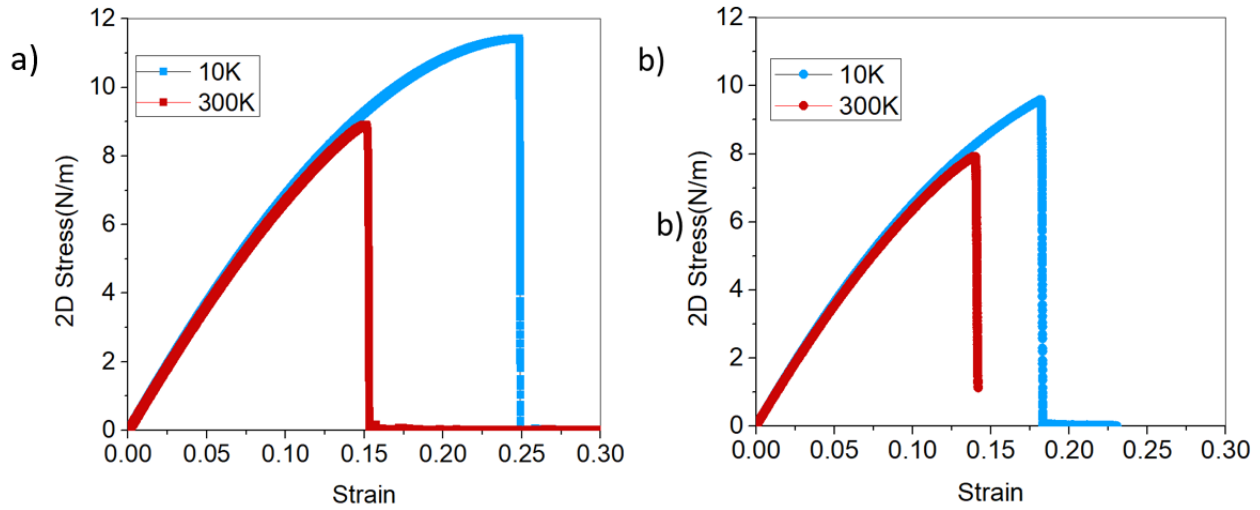


Figure 4: Stress-strain curve of a monolayer MoTe₂ under uniaxial tension along (a) armchair and (b) zigzag directions at 10K and 300K.

Next, we investigate the effect of varying temperatures on the physical properties of 2D MoTe₂ under uniaxial tension. In addition to our simulations at temperatures 10K and 300K, we also simulated the fracture behavior for 100K to 600K temperatures. The temperature showed a significant impact on the physical properties of 2D sheets. The stress-strain relationships are illustrated in Figure 5.

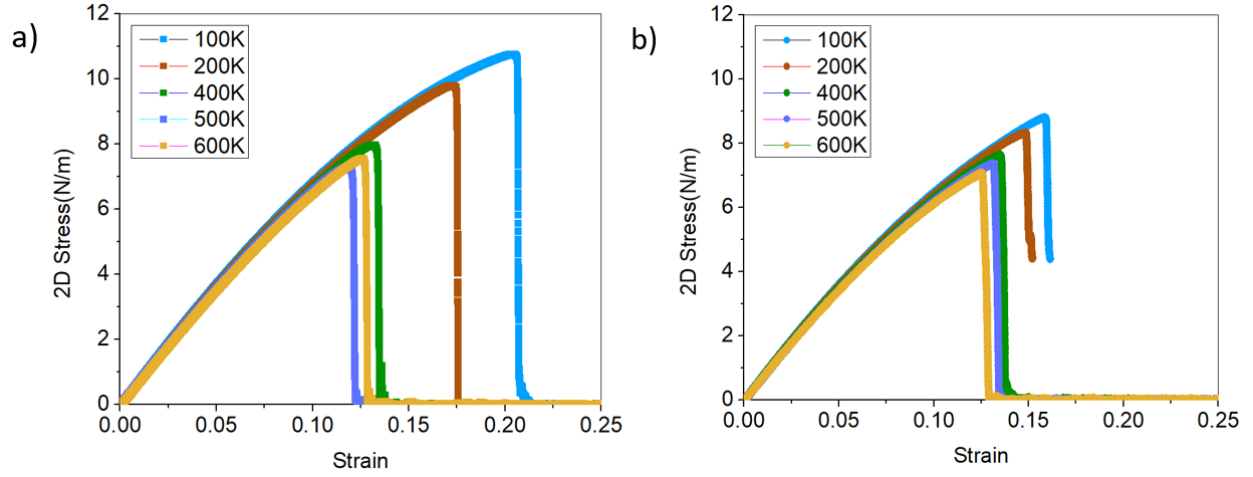


Figure 5: Stress-strain curve of a monolayer MoTe_2 under uniaxial tension along (a) armchair and (b) zigzag directions at different temperatures.

Note that even at elevated temperatures, the 2D sheet undergoes a brittle fracture without showing any sign of plastic deformation. Figure 5 also shows that the ultimate strain falls with increasing temperature due to the presence of high thermal vibrations [41]. The fracture strength of MoTe_2 was reduced by $\sim 34\%$ and $\sim 26\%$ in the armchair and zigzag direction, respectively with the increase of temperature. The fracture strain was reduced by $\sim 49.5\%$ and $\sim 31\%$ in the armchair and zigzag directions, respectively. The relation between the 3D young's modulus, 3D fracture strength, fracture strain, and temperature are shown in Figure 6 (a-c).

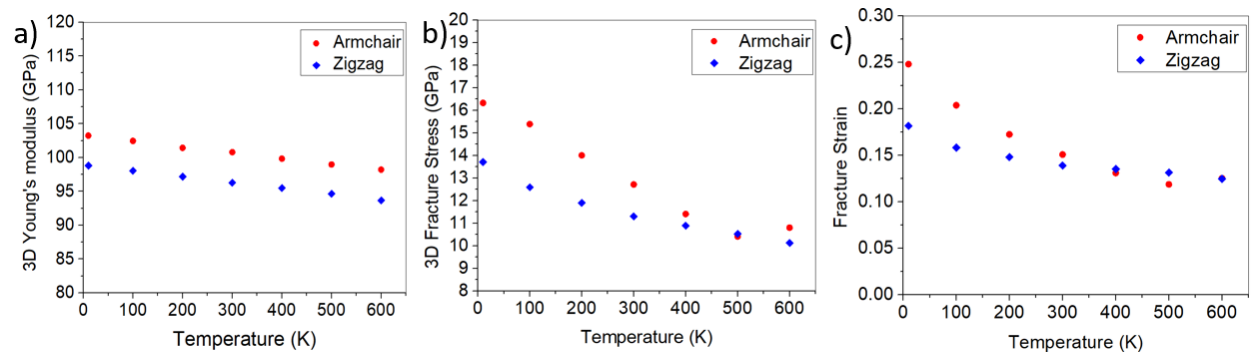


Figure 6: (a) Elastic modulus, (b) Fracture strength, and (c) Fracture strain of monolayer MoTe_2 at different temperatures.

4. Conclusion

The fracture behaviors of a monolayer of molybdenum ditelluride (2H-MoTe₂) has been investigated using molecular dynamics simulations. The fracture test was simulated under varying temperatures for both armchair and zigzag directions. And our conclusion are:

- (a) Temperature plays a significant role of the fracture mechanics of MoTe₂. The stress-strain plot depicts that their property diminished with increasing temperatures. This is an important consideration when applying these 2D materials for high temperature applications.
- (b) The visual results of simulation reveal the difference in crack formation patterns for armchair and zigzag directions. Uniaxial stress in armchair directions projects a clean and fine crack on the sheet. Whereas, the same stress applied to zigzag direction initiated multiple distorted cracks.
- (c) It is found that the Young's Modulus, fracture strain and fracture strain are strongly anisotropic.

Author contributions: A.S.M and A.F.A modeled the experiments in the simulator and conducted the experiments. A.S.M and A.F.A wrote the manuscript. M.T.F and R.A.S helped to run the simulations. S.S, Y.A, M.R.K, M.T.F and M.A.I helped to review the manuscript. S.S, Y.A, M.R.K, M.T.F and M.A.I supervised the work. All authors discussed the results and reviewed the final manuscript. **Competing interests:** The authors declare that they have no competing interests. **Data and materials availability:** All data needed to evaluate the conclusions in the paper are present in the paper. Additional data related to this paper may be requested from the authors.

Acknowledgement: The authors would like to acknowledge Prof. Jin-Wu Jiang from Shanghai Institute of Applied Mathematics and Mechanics, Shanghai University, for his valuable guidance and support.

5. References:

- [1] K. S. Novoselov *et al.*, “Two-dimensional gas of massless Dirac fermions in graphene,” *Nature*, vol. 438, no. 7065, pp. 197–200, Nov. 2005, doi: 10.1038/nature04233.
- [2] C. Lee, X. Wei, J. W. Kysar, and J. Hone, “Measurement of the elastic properties and intrinsic strength of monolayer graphene,” *Science (1979)*, vol. 321, no. 5887, pp. 385–388, Jul. 2008, doi: 10.1126/SCIENCE.1157996/SUPPL_FILE/LEE-SOM.PDF.
- [3] B. Uchoa and A. H. Castro Neto, “Superconducting states of pure and doped graphene,” *Phys Rev Lett*, vol. 98, no. 14, 2007, doi: 10.1103/PhysRevLett.98.146801.
- [4] A. A. Balandin *et al.*, “Superior thermal conductivity of single-layer graphene,” *Nano Lett*, vol. 8, no. 3, pp. 902–907, Mar. 2008, doi: 10.1021/NL0731872/ASSET/IMAGES/MEDIUM/NL-2007-031872_0005.GIF.
- [5] L. A. Falkovsky and L. D. Landau, “Optical properties of graphene,” *J Phys Conf Ser*, vol. 129, no. 1, p. 012004, Oct. 2008, doi: 10.1088/1742-6596/129/1/012004.
- [6] A. Varykhalov *et al.*, “Electronic and magnetic properties of quasifreestanding graphene on Ni,” *Phys Rev Lett*, vol. 101, no. 15, p. 157601, Oct. 2008, doi: 10.1103/PHYSREVLETT.101.157601/FIGURES/4/MEDIUM.
- [7] C. Deepa, L. Rajeshkumar, and M. Ramesh, “Preparation, synthesis, properties and characterization of graphene-based 2D nano-materials for biosensors and bioelectronics,” *Journal of Materials Research and Technology*, vol. 19, pp. 2657–2694, Jul. 2022, doi: 10.1016/J.JMRT.2022.06.023.
- [8] X. Su *et al.*, “Bandgap engineering of MoS₂/MX₂ (MX₂ = WS₂, MoSe₂ and WSe₂) heterobilayers subjected to biaxial strain and normal compressive strain,” *RSC Adv*, vol. 6, no. 22, pp. 18319–18325, Feb. 2016, doi: 10.1039/C5RA27871F.
- [9] H. J. Conley, B. Wang, J. I. Ziegler, R. F. Haglund, S. T. Pantelides, and K. I. Bolotin, “Bandgap engineering of strained monolayer and bilayer MoS₂,” *Nano Lett*, vol. 13, no. 8, pp. 3626–3630, Aug. 2013, doi: 10.1021/NL4014748/SUPPL_FILE/NL4014748_SI_001.PDF.
- [10] D. Braga, I. Gutiérrez Lezama, H. Berger, and A. F. Morpurgo, “Quantitative determination of the band gap of WS₂ with ambipolar ionic liquid-gated transistors,” *Nano Lett*, vol. 12, no. 10, pp. 5218–5223, Oct. 2012, doi: 10.1021/NL302389D/SUPPL_FILE/NL302389D_SI_001.PDF.
- [11] G. Eda, T. Fujita, H. Yamaguchi, D. Voiry, M. Chen, and M. Chhowalla, “Coherent atomic and electronic heterostructures of single-layer MoS₂,” *ACS Nano*, vol. 6, no. 8, pp. 7311–7317, Aug. 2012, doi: 10.1021/NN302422X/ASSET/IMAGES/MEDIUM/NN-2012-02422X_0002.GIF.
- [12] A. N. Enyashin *et al.*, “New route for stabilization of 1T-WS₂ and MoS₂ phases,” *Journal of Physical Chemistry C*, vol. 115, no. 50, pp. 24586–24591, Dec. 2011, doi: 10.1021/JP2076325/ASSET/IMAGES/MEDIUM/JP-2011-076325_0006.GIF.

- [13] J. A. Wilson and A. D. Yoffe, "The transition metal dichalcogenides discussion and interpretation of the observed optical, electrical and structural properties," *Adv Phys*, 1969, doi: 10.1080/00018736900101307.
- [14] D. Voiry *et al.*, "Enhanced catalytic activity in strained chemically exfoliated WS₂ nanosheets for hydrogen evolution," *Nat Mater*, vol. 12, no. 9, pp. 850–855, 2013, doi: 10.1038/NMAT3700.
- [15] D. Voiry *et al.*, "Conducting MoS₂ nanosheets as catalysts for hydrogen evolution reaction," *Nano Lett*, vol. 13, no. 12, pp. 6222–6227, Dec. 2013, doi: 10.1021/NL403661S/SUPPL_FILE/NL403661S_SI_001.PDF.
- [16] M. A. Lukowski, A. S. Daniel, F. Meng, A. Forticaux, L. Li, and S. Jin, "Enhanced hydrogen evolution catalysis from chemically exfoliated metallic MoS₂ nanosheets," *J Am Chem Soc*, vol. 135, no. 28, pp. 10274–10277, Jul. 2013, doi: 10.1021/JA404523S/SUPPL_FILE/JA404523S_SI_001.PDF.
- [17] K.-A. N. Duerloo, Y. Li, and E. J. Reed, "Structural phase transitions in two-dimensional Mo- and W-dichalcogenide monolayers," *Nat Commun*, vol. 5, no. 1, p. 4214, Sep. 2014, doi: 10.1038/ncomms5214.
- [18] S. Cho *et al.*, "Phase patterning for ohmic homojunction contact in MoTe₂," *Science (1979)*, vol. 349, no. 6248, pp. 625–628, Aug. 2015, doi: 10.1126/SCIENCE.AAB3175/SUPPL_FILE/CHO-SM.PDF.
- [19] C. Ruppert, O. B. Aslan, and T. F. Heinz, "Optical properties and band gap of single- and few-layer MoTe₂ crystals," *Nano Lett*, vol. 14, no. 11, pp. 6231–6236, Nov. 2014, doi: 10.1021/NL502557G/SUPPL_FILE/NL502557G_SI_001.PDF.
- [20] Y. Q. Bie *et al.*, "A MoTe₂-based light-emitting diode and photodetector for silicon photonic integrated circuits," *Nature Nanotechnology 2017 12:12*, vol. 12, no. 12, pp. 1124–1129, Oct. 2017, doi: 10.1038/nnano.2017.209.
- [21] B. Yu *et al.*, "Outstanding Catalytic Effects of 1T'-MoTe₂Quantum Dots@3D Graphene in Shuttle-Free Li-S Batteries," *ACS Nano*, vol. 15, no. 8, pp. 13279–13288, Aug. 2021, doi: 10.1021/ACSNANO.1C03011/SUPPL_FILE/NN1C03011_SI_001.PDF.
- [22] S. Kang *et al.*, "Tunable Out-of-Plane Piezoelectricity in Thin-Layered MoTe₂ by Surface Corrugation-Mediated Flexoelectricity," *ACS Appl Mater Interfaces*, vol. 10, no. 32, pp. 27424–27431, Aug. 2018, doi: 10.1021/ACSAMI.8B06325/SUPPL_FILE/AM8B06325_SI_001.PDF.
- [23] Y. Tan *et al.*, "Controllable 2H-to-1T' phase transition in few-layer MoTe₂," *Nanoscale*, vol. 10, no. 42, pp. 19964–19971, Nov. 2018, doi: 10.1039/C8NR06115G.
- [24] S. A. Chowdhury *et al.*, "Mechanical Properties and Strain Transfer Behavior of Molybdenum Ditelluride (MoTe₂) Thin Films," *J Eng Mater Technol*, vol. 144, no. 1, pp. 1–10, 2022, doi: 10.1115/1.4051306.
- [25] H. Cheong, Y. Cheon, S. Y. Lim, and K. Kim, "Structural phase transition and interlayer coupling in few-layer 1t' and td mote₂," *ACS Nano*, vol. 15, no. 2, pp. 2962–2970, Feb. 2021, doi: 10.1021/ACSNANO.0C09162/SUPPL_FILE/NN0C09162_SI_001.PDF.

- [26] D. Vikraman *et al.*, “Fullerene-free, MoTe₂ atomic layer blended bulk heterojunctions for improved organic solar cell and photodetector performance,” *Journal of Materials Research and Technology*, vol. 17, pp. 2875–2887, Mar. 2022, doi: 10.1016/J.JMRT.2022.02.050.
- [27] Y. Sun *et al.*, “Elastic Properties and Fracture Behaviors of Biaxially Deformed, Polymorphic MoTe₂,” *Nano Lett*, vol. 19, no. 2, pp. 761–769, 2019, doi: 10.1021/acs.nanolett.8b03833.
- [28] S. Song, D. H. Keum, S. Cho, D. Perello, Y. Kim, and Y. H. Lee, “Room Temperature Semiconductor-Metal Transition of MoTe₂ Thin Films Engineered by Strain,” *Nano Lett*, vol. 16, no. 1, 2016, doi: 10.1021/acs.nanolett.5b03481.
- [29] G. Mirabelli *et al.*, “Air sensitivity of MoS₂, MoSe₂, MoTe₂, HfS₂, and HfSe₂,” *J Appl Phys*, vol. 120, no. 12, p. 125102, Sep. 2016, doi: 10.1063/1.4963290.
- [30] B. Mortazavi, G. R. Berdiyorov, M. Makaremi, and T. Rabczuk, “Mechanical responses of two-dimensional MoTe₂; pristine 2H, 1T and 1T' and 1T'/2H heterostructure,” *Extreme Mech Lett*, vol. 20, pp. 65–72, Apr. 2018, doi: 10.1016/J.EML.2018.01.005.
- [31] M. Q. Le, “Fracture and strength of single-atom-thick hexagonal materials,” *Comput Mater Sci*, vol. 201, p. 110854, Jan. 2022, doi: 10.1016/J.COMMATSCI.2021.110854.
- [32] M. A. Torkaman-Asadi and M. A. Kouchakzadeh, “Atomistic simulations of mechanical properties and fracture of graphene: A review,” *Comput Mater Sci*, vol. 210, p. 111457, Jul. 2022, doi: 10.1016/J.COMMATSCI.2022.111457.
- [33] D. Puotinen, R. E. Newnham, and IUCr, “The crystal structure of MoTe₂,” *urn:issn:0365-110X*, vol. 14, no. 6, pp. 691–692, Jun. 1961, doi: 10.1107/S0365110X61002084.
- [34] A. P. Thompson *et al.*, “LAMMPS - a flexible simulation tool for particle-based materials modeling at the atomic, meso, and continuum scales,” *Comput Phys Commun*, vol. 271, p. 108171, Feb. 2022, doi: 10.1016/j.cpc.2021.108171.
- [35] J.-W. Jiang and Y.-P. Zhou, “Parameterization of Stillinger-Weber Potential for Two-Dimensional Atomic Crystals,” in *Handbook of Stillinger-Weber Potential Parameters for Two-Dimensional Atomic Crystals*, InTech, 2017, p. 13. doi: 10.5772/intechopen.71929.
- [36] J.-W. Jiang, “Parametrization of Stillinger–Weber potential based on valence force field model: application to single-layer MoS₂ and black phosphorus,” *Nanotechnology*, vol. 26, no. 31, p. 315706, Jul. 2015, doi: 10.1088/0957-4484/26/31/315706.
- [37] J.-W. Jiang, “Misfit Strain-Induced Buckling for Transition-Metal Dichalcogenide Lateral Heterostructures: A Molecular Dynamics Study,” *Acta Mechanica Sinica*, vol. 32, no. 1, pp. 17–28, Feb. 2019, doi: 10.1007/s10338-018-0049-z.
- [38] M. M. Islam *et al.*, “ReaxFF molecular dynamics simulations on lithiated sulfur cathode materials,” *Physical Chemistry Chemical Physics*, vol. 17, no. 5, pp. 3383–3393, 2015, doi: 10.1039/C4CP04532G.
- [39] R. A. S. I. Subad, T. S. Akash, P. Bose, and M. M. Islam, “Engineered defects to modulate fracture strength of single layer MoS₂: An atomistic study,” *Physica B Condens Matter*, vol. 592, no. October 2019, p. 412219, Sep. 2020, doi: 10.1016/j.physb.2020.412219.

- [40] T. Li, “Ideal strength and phonon instability in single-layer MoS₂,” *Phys Rev B Condens Matter Mater Phys*, vol. 85, no. 23, p. 235407, Jun. 2012, doi: 10.1103/PHYSREVB.85.235407/FIGURES/5/MEDIUM.
- [41] J. W. Jiang and H. S. Park, “Mechanical properties of MoS₂/graphene heterostructures,” *Appl Phys Lett*, vol. 105, no. 3, p. 033108, Jul. 2014, doi: 10.1063/1.4891342.